Journal of Materials Science and Engineering B 10 (5-6) (2020) 85-105
doi: 10.17265/2161-6221/2020.5-6.001

Performance Characterization of Modified ASTM F75 Alloy for Hip Implant Application

Patrick F. Yao, Siqi Li and Rong Liu

Department of Mechanical and Aerospace Engineering, Carleton University, 1125 Colonel by Drive, Ottawa, Ontario, Canada K1S 5B6, Canada

Abstract: ASTM F75 is a low-carbon CoCrMo alloy which has been used as hip implant material for decades, but the ASTM F75 implants can fail when the femoral head and the acetabular cup loosen because of limited metal-on-metal bearing. Therefore, a modified version of ASTM F75 alloy which has 90 wt.% ASTM F75 plus 10 wt.% Cr is proposed. The wear and corrosion resistance of both alloys are investigated simulating the working environment of hip implants in human body. The mechanics behavior of the femoral implant under the loading condition in human body with ASTM F75 or modified ASTM F75 material used is studied with FEA simulation. The cytotoxicity (MTT) assays of the alloys are measured and compared to that of inert ceramic and cytotoxic cobalt. The experimental and simulation results show that the proposed alloy exhibits better wear and corrosion resistance than the conventional hip implant material. Both alloys behave well with respect to stress and deformation when used for the femoral implant under the loading condition in human body. These two alloys display similar cytotoxicity performance to inert ceramic.

Key words: Hip implant, modified ASTM F75 alloy, stress, wear, corrosion.

1. Introduction

As a common intervention for arthritis and rheumatism, total hip arthroplasty is a surgical reconstruction of the hip joint with an artificial prosthetic. Total hip replacement has been shown to improve functional status and relieve the pain often associated with osteoarthritis, rheumatoid arthritis and traumatic arthritis [1]. The hip replacement prosthesis is made up of two main parts, the femoral and acetabular components. The modern femoral implant consists of femoral head and stem components, as shown in Fig. 1.

Femoral head is the part of the femoral component that interfaces with the acetabular cup. It is typically made of metal. The main requirements of the femoral head component include extremely low roughness, high hardness, good wear and corrosion resistance, and non-cytotoxic property of released ions/debris [2]. The femoral head must have extremely low average roughness as it reduces the wear rate of the surface. High hardness also plays a part in increasing the surfaces wear resistance subsequently minimizing metal ion release [3]. Aseptic loosening usually occurs when wear particles form at the bearing surfaces of the implant due to friction at the joint, which induces biological responses and causes osteolysis. These wear particles are composed of microscopic grains of bearing material [4]. Another crucial property of femoral head is that the metal ions released should be non-toxic. Cytotoxicity of released metallic ions can affect the surrounding tissue thus leading to the loosening of the implant. Other necessary properties crucial in bearing surfaces include good fracture toughness, yield strength and density [5].

The femoral stem is part of the prosthesis that fits into the femur (thigh bone). Bone is firstly removed from the femur and shaped to fit the dimensions of the stem. The fixation is normally cemented [6]. The stem is made of metallic alloys mainly titanium based, cobalt chrome alloys and 316L stainless steel [7]. The main requirements for femoral stems include excellent

Corresponding author: Rong Liu, PhD, professor, research fields: superalloys, surface coatings, fracture mechanics.

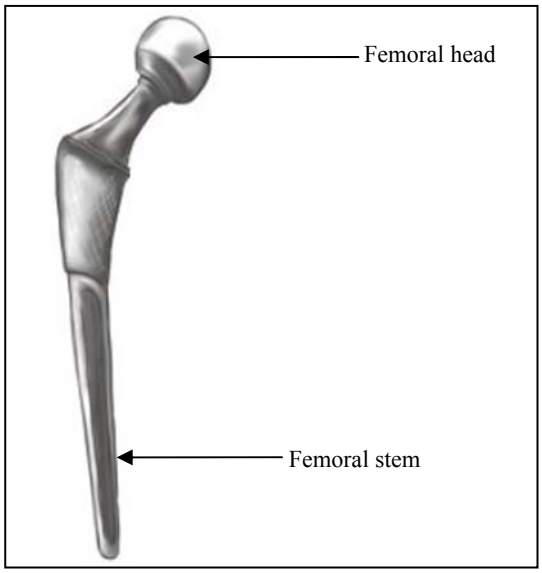

Fig. 1 A typical femoral implant of hip replacement.

osseointegration, high wear and corrosion resistance. Osseointegration refers to the direct structural and functional connection between living bone and the surface of a load-bearing artificial implant without intervening connective tissue. The implant material has to permit bone cells to attach and proliferate on the surface without imposing cytotoxic risks [8]. Wear accelerated by corrosion also plays a part in the mechanical degradation. This type of corrosive degradation can progress little by little for many years on the surface of material attaching to the surrounding tissue [9]. Other properties necessary in femoral stem requirements include low elastic modulus (close to bone in order to prevent stress shielding), high strength, good fatigue resistance and good fracture toughness [10].

From the mechanical and chemical standpoint, cobalt-chromium-molybdenum (CoCrMo) alloys have historically been a popular choice for hip implants owing to their good wear and corrosion resistance. The typical CoCrMo alloy in medical application, known as ASTM F75 or the medical version of Stellite 21, is one of the most popular materials used for femoral implants, owing to excellent mechanical and tribological properties and corrosion resistance [11]. It is a better option for metal-on-metal bearing components of orthopedic implants when compared with stainless steels and titanium alloys [12]. The chromium can form Cr-rich oxide films on the alloy surface *in vivo*, which affords excellent corrosion resistance [13]. The mechanical strength and wear resistance of ASTM F75 are enhanced by formation of Cr-rich carbides and strengthened solid solution matrix, which results in less wear debris, compared to other competing alloys.

ASTM F75 has been long used for hip implants, however, it was found that after long-time service loosening of the femoral head and the cup occurred [14]. In some cases, the metallic wear debris from the implants has induced osteolytic and cytotoxic responses [15]. Also, the metal ions can increase the risk of implant failure by inducing hypersensitivity [16]. In addition, volumetric wear rate of the metal surface is strongly related to the levels of metallic ions. Although there have been no systemic studies on side effects or limits to the amount of the wear/corrosion products that can be tolerated by the body, there is general consensus to find ways to reduce wear, wear debris, and corrosion ion release [17].

Therefore, a modified ASTM F75 has been proposed, with addition of extra Cr, in order to improve metal-on-metal bearing performance. In this research the wear resistance of ASTM F75 and the modified version were evaluated on a tribometer in dry-sliding mode. The corrosion behavior of the alloys was investigated and compared under electrochemical and immersion tests in Hank's solution at 37 °C, which simulated the human body fluid environment. The mechanics performance of the femoral implant made of ASTM F75 or modified ASTM F75 was studied under the working condition in the human body using finite element analysis (FEA). The cytotoxicity responses of the alloys were measured. The outcomes of this research will provide the prosthesis industry the scientific evidence for using improved hip implant material with extended service life.

2. Alloy Specimens

2.1 Composition and Mechanical Properties

The ASTM F75 alloy specimens were cast products but the modified ASTM F75 alloy specimens were processed via hot isostatic pressing (HIP), since this means eased fabricating the modified ASTM F75 alloy by adding Cr powder into ASTM F75 powder. The chemical compositions (wt.%) of the alloys are detailed in Table 1. Addition of extra Cr in modified ASTM F75 was to enhance the solid solution matrix for wear resistance and mechanical strength. The mechanical properties of the alloys are given in Table 2.

2.2 Microstructure and Phases

The microstructures of ASTM F75 and modified ASTM F75 were examined using SEM/EDS. As shown in Fig. 2, ASTM F75 alloy consists of primary Co solid solution with minor carbides precipitated in the eutectic phase. Since ASTM F75 contains a very low level of C (0.25 wt.%), the volume fraction of carbides in this alloy is only about 4% [18]. Therefore, ASTM F75 is a solution-strengthened alloy rather than a carbide-strengthened alloy. Furthermore, EDX analysis was conducted on the solid solution phase and the fishbone eutectic phase (carbides and Co solid solution mixture) of the alloy. As illustrated in Fig. 3, the solid solution contains very high Co content and also some Cr and Mo while the eutectic phase has high C and very high Cr so that the carbide in this alloy should be $Cr_{23}C_6$ instead of Cr_7C_3. It has been reported in Ref. [19] that $Cr_{23}C_6$ is commonly abundant in low-carbon cobalt-based alloys. There is also high Co content in the eutectic phase which comes from the Co solid solution.

Table 1 Chemical compositions (wt.%) of the alloys under study.

Alloy	Co	Cr	Mo	Ni	C
ASTM F75	Balance	27	5.5	0.5	0.25
Modified ASTM F75	Balance	35	5.0	0.5	0.23

Table 2 Mechanical properties of the alloys under study.

Alloy	Density (g/cm^2)	Young's modulus (GPa)	Poisson ratio	Yield stress (MPa)	Ultimate strength (MPa)
ASTM F75	8.3	220	0.3	450	655
Modified ASTM F75	8.3	210	0.3	633	868

Table 3 Chemical composition of Hank's solution.

Chemical	Concentration (g/L)
NaCl	8.00
KCl	0.40
$MgSO_4 \cdot 7H_2O$	0.049
$MgCl_2 \cdot 6H_2O$	0.10
$CaCl_2 \cdot 2H_2O$	0.185
$Na_2HPO_4 \cdot 12H_2O$	0.121
KH_2PO_4	0.06
$NaHCO_3$	0.35
Glucose	1.00

The SEM microstructure and EDX spectra along with elemental content tables for modified ASTM F75 alloy are presented in Figs. 4 and 5. Similar to ASTM F75, the microstructure of modified ASTM F75 also contains the primary Co solid solution phase and the eutectic phase ($Cr_{23}C_6$ carbide + Co solid solution). Differently, the eutectic phase of modified ASTM F75 is finer and the carbide size is much smaller (Fig. 4) when compared to that in ASTM F75. The amount of carbides is also reduced in this alloy. These can be attributed to the solidus nature of HIP process. The EDX results in Fig. 5 confirm that the Cr content in the solid solution of modified ASTM F75 is much higher than that in the solid solution of ASTM F75. This is due to the addition of extra Cr in the former.

3. Wear and Corrosion Experiments

3.1 Pin-on-Disk Wear Test

The wear resistance of ASTM F75 and modified ASTM F75 was evaluated using a Neoplus pin-on-disk tribometer in dry-sliding mode. The apparatus used a rotating pin that pressed perpendicularly against a static disk (the specimen 12 × 12 × 4 mm) under a constant normal force, which was adjusted by a two-stage lever and attached weights. The pin was a

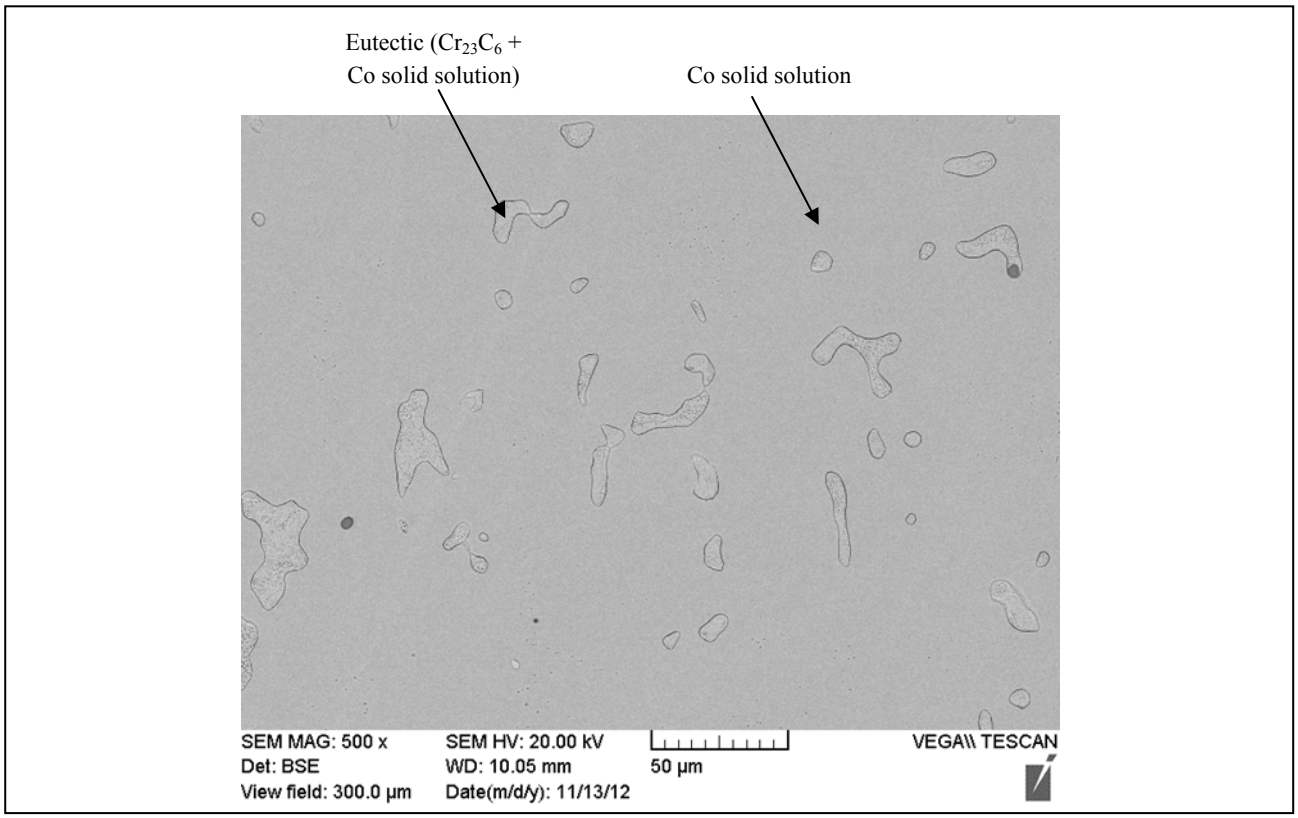

(a)

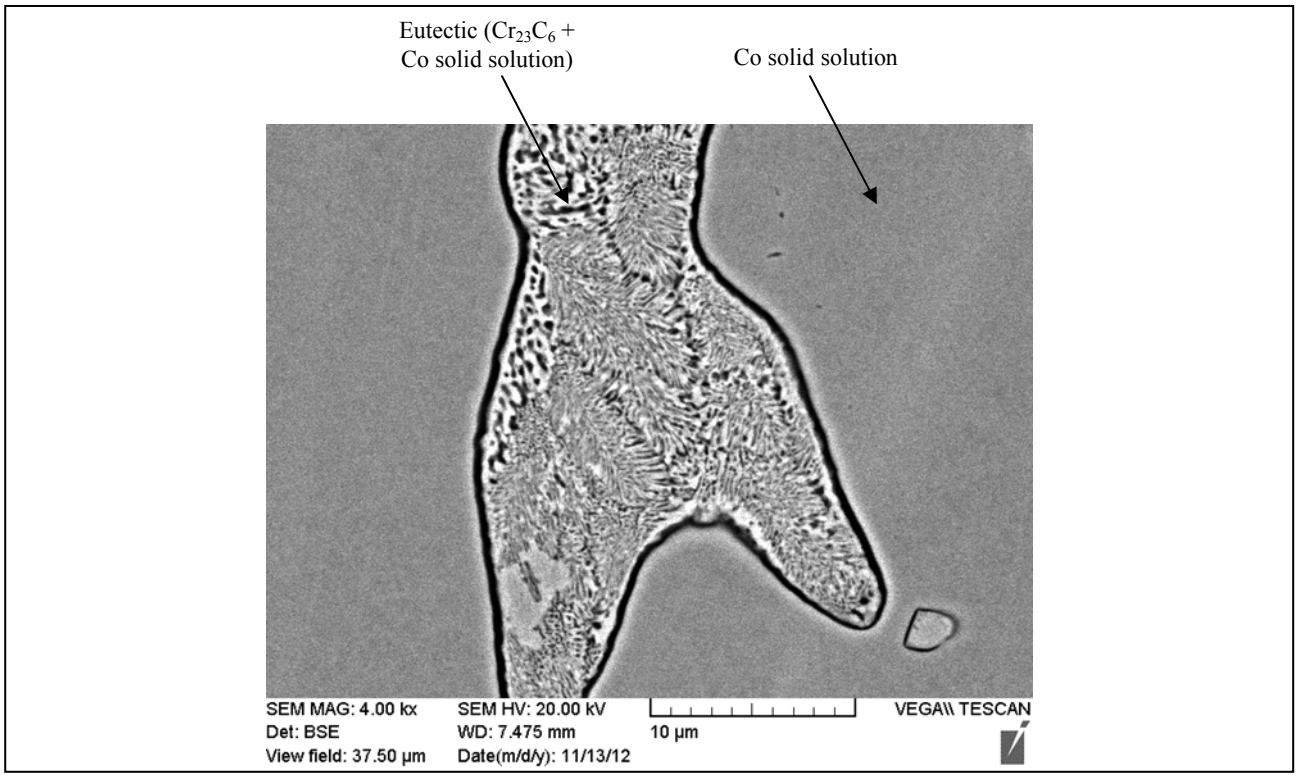

(b)

Fig. 2 SEM microstructure of ASTM F75: (a) at low magnification and (b) at high magnification.

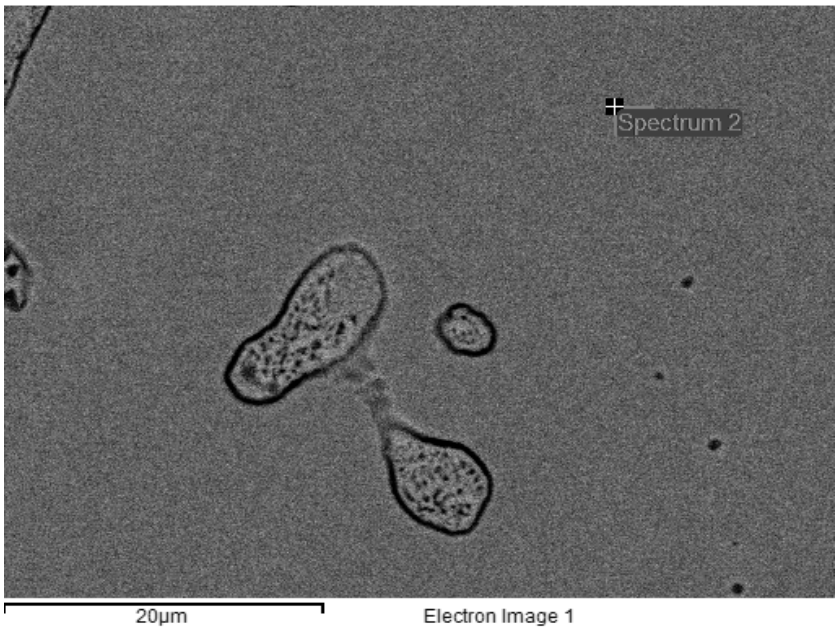

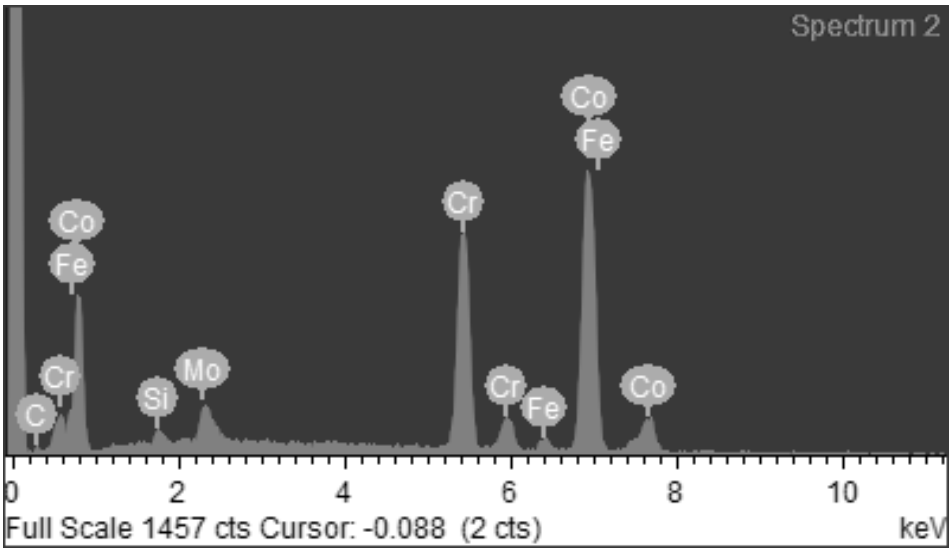

Element	wt.%	at.%
Si K	0.79	1.62
Cr K	27.69	30.8
Fe K	2.08	2.13
Co K	64.17	62.51
Mo L	5.27	3.15
Totals	100	100

(a)

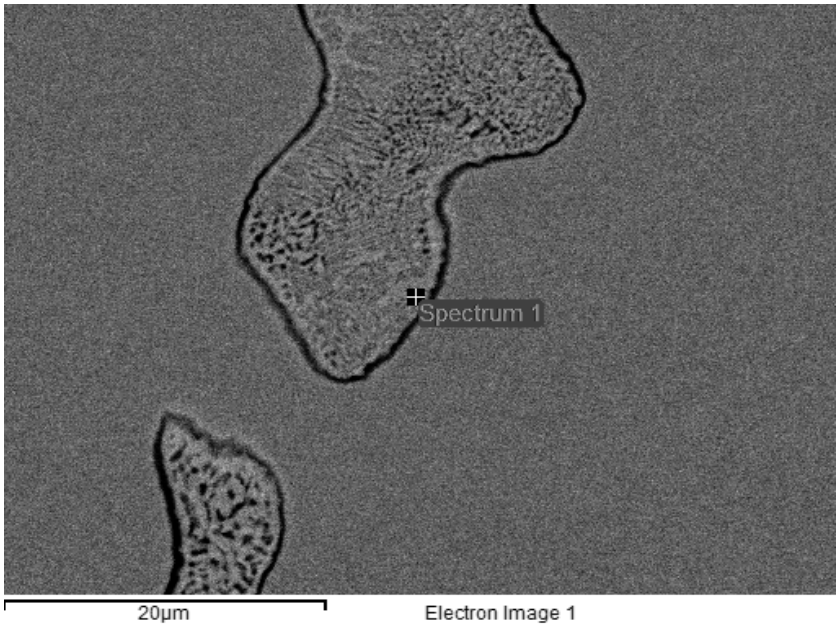

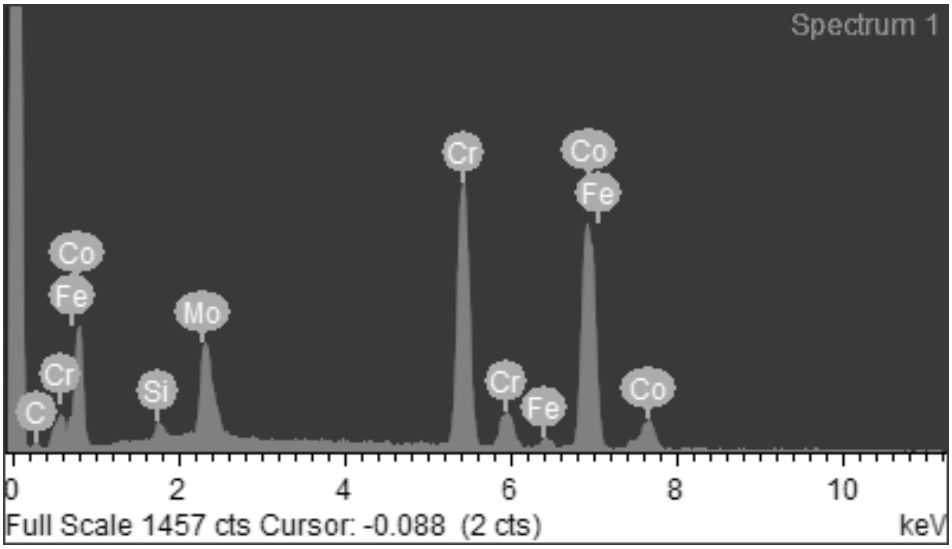

Element	wt.%	at.%
Si K	0.79	1.71
Cr K	32.97	37.32
Fe K	1.72	1.80
Co K	50.86	50.80
Mo L	13.16	8.37
Totals	100	100

(b)

Fig. 3 EDX results of ASTM F75: (a) Co solid solution and (b) eutectic ($Cr_{23}C_6$ carbide and Co solid solution).

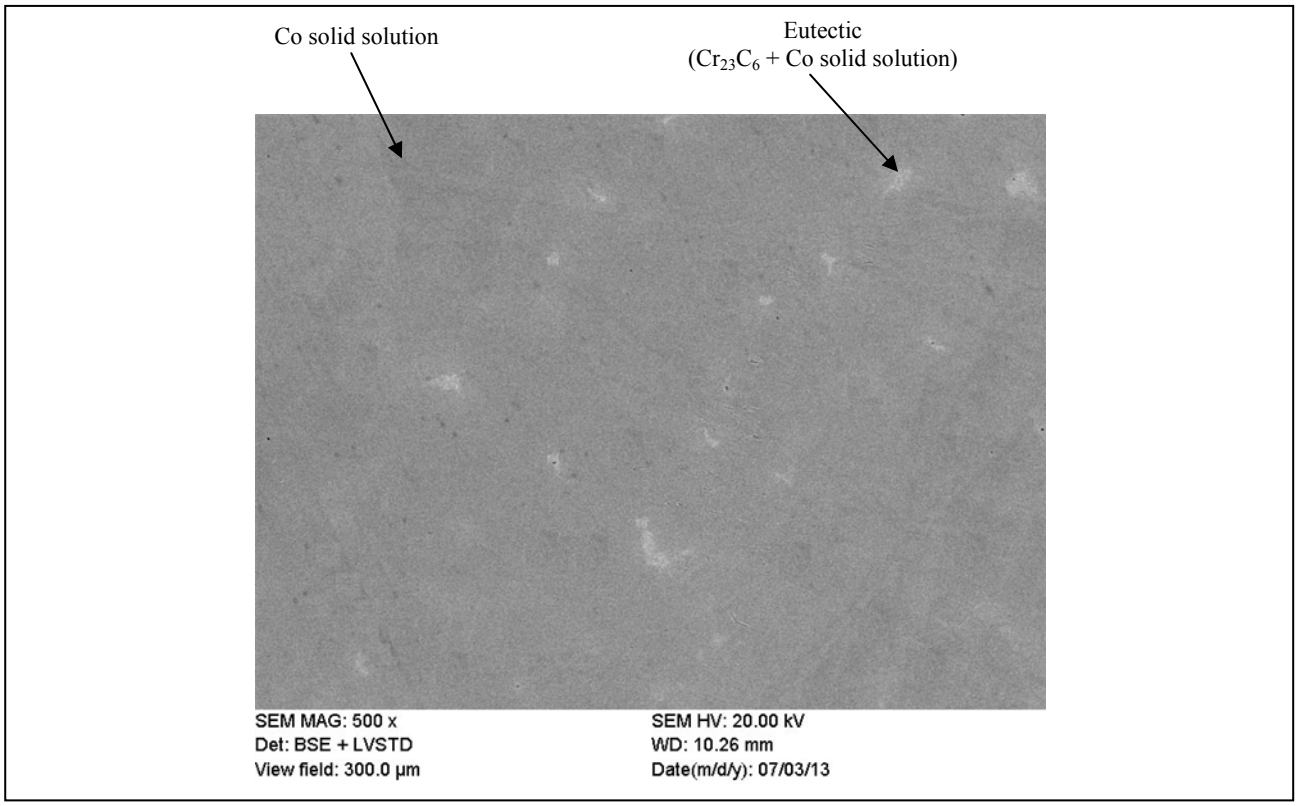

(a)

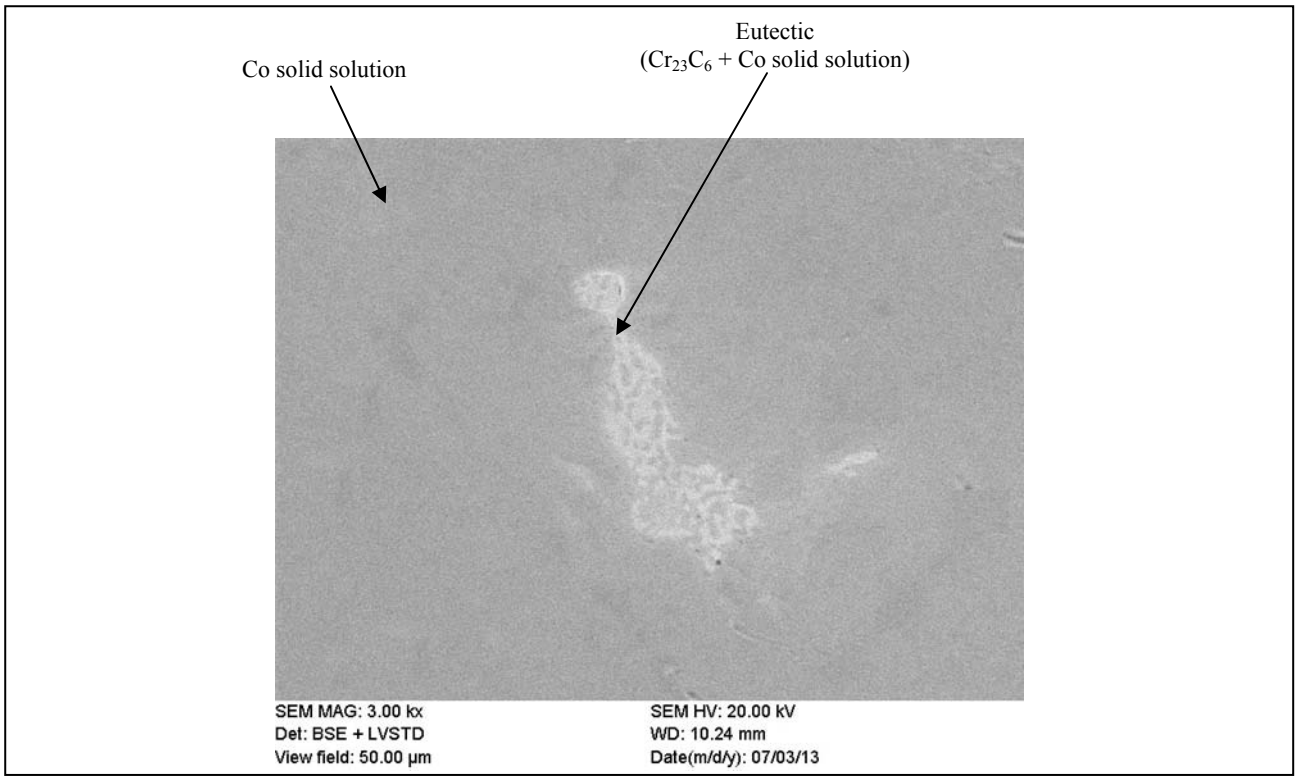

(b)

Fig. 4 SEM microstructure of modified ASTM F75: (a) at low magnification and (b) at high magnification.

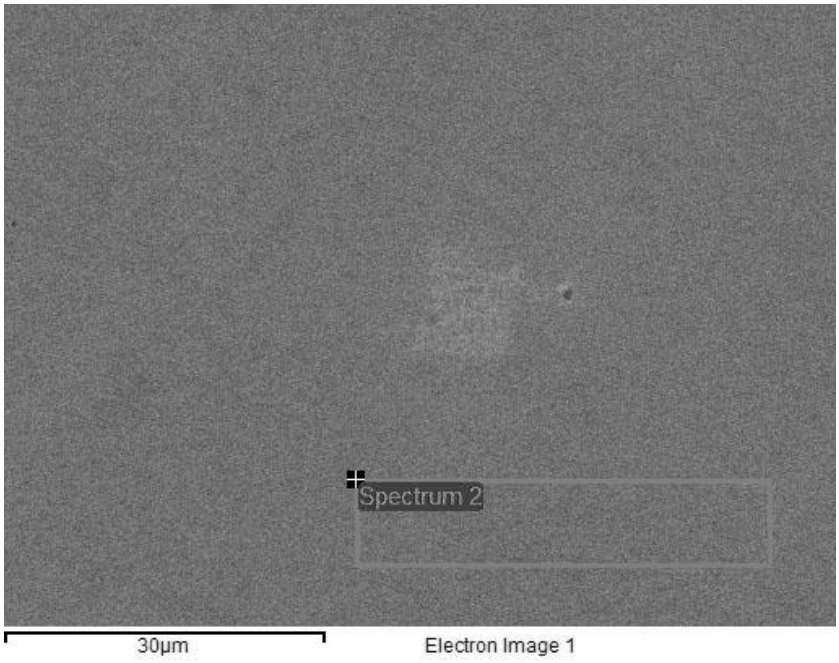

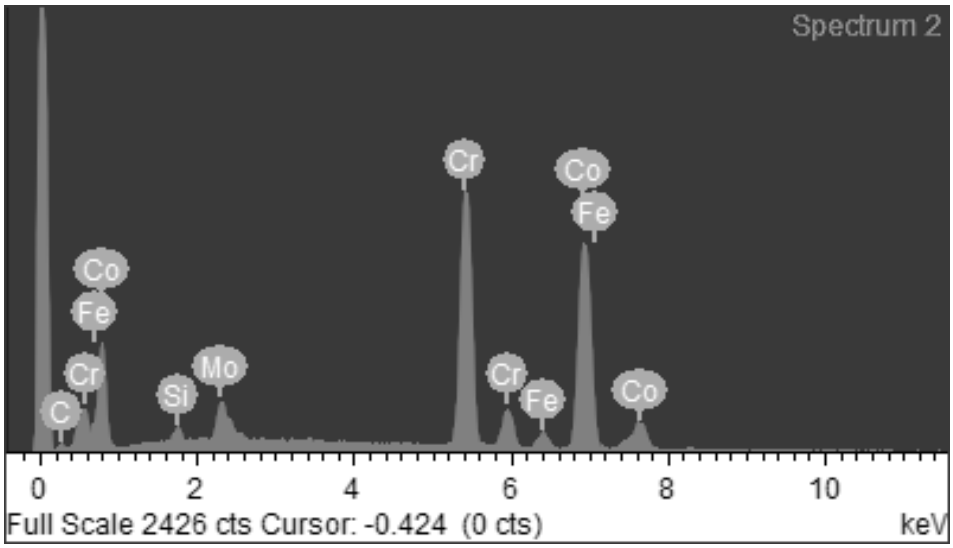

Element	wt.%	at.%
Si K	0.88	1.75
Cr K	36.38	39.73
Fe K	3	3.05
Co K	54.12	52.14
Mo L	5.62	3.33
Totals	100	100

(a)

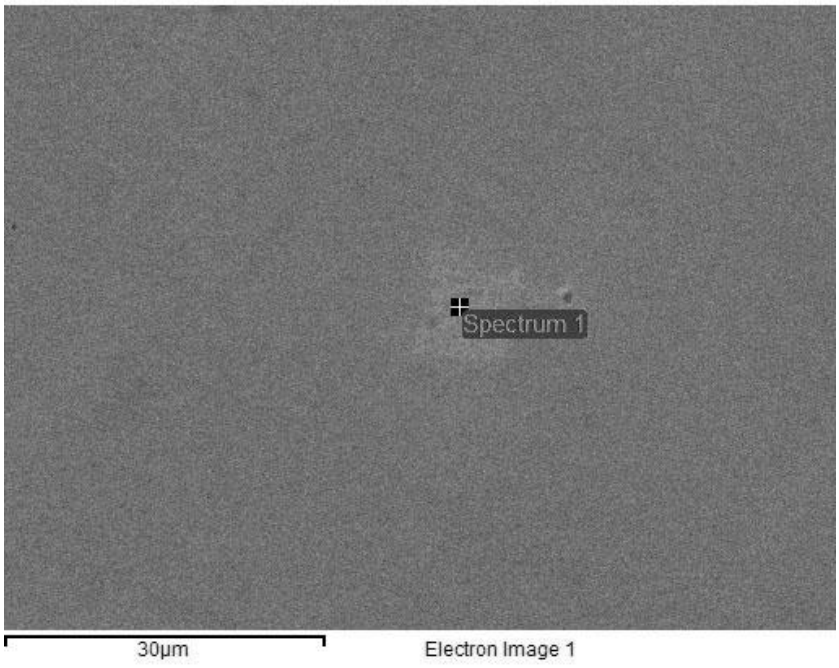

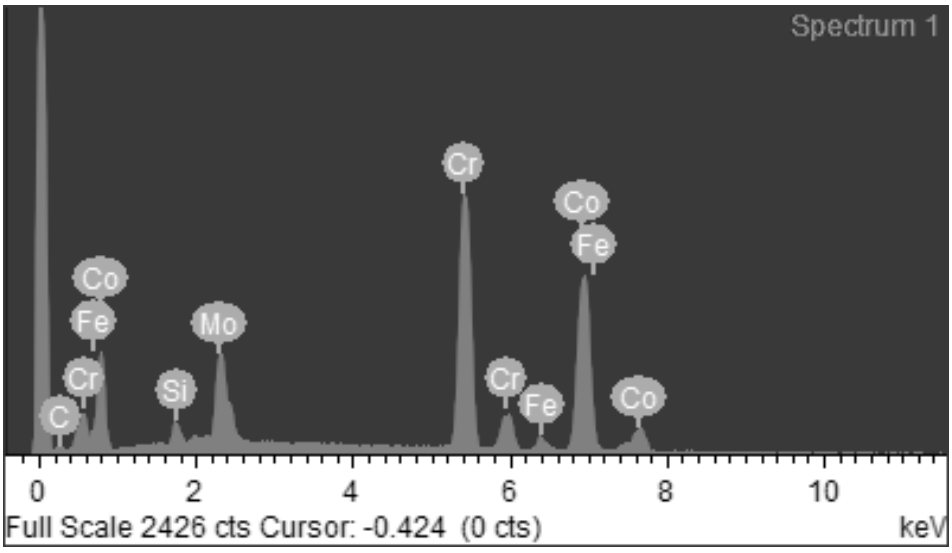

Element	wt.%	at.%
Si K	1.31	2.71
Cr K	36.79	41.18
Fe K	2.39	2.49
Co K	45.98	45.41
Mo L	13.53	8.21
Totals	100	100

(b)

Fig. 5 EDX results of modified ASTM F75: (a) Co solid solution and (b) eutectic ($Cr_{23}C_6$ carbide and Co solid solution).

ball of radius 2.5 mm made of 94 wt.% WC and 6 wt.% Co with the Vickers hardness of HV1534. The apparatus recorded the sliding distance, friction force, and friction coefficient with time. The test was conducted at room temperature with no lubrication. A normal force of 5 N was applied against the ball and disk (specimen). The pin (ball) was placed at a distance of 3 mm away from the rotation center, which had a rotational speed of 350 rpm, corresponding to a sliding speed of 110 mm/s. The interacting result was a 6 mm diameter circular wear track in the disk test specimen surface. The test duration was 2.5 h, which resulted in a total sliding length of 990 m. Three specimens were tested for each alloy under the same condition to verify the wear loss results.

3.2 Hank's Solution

The corrosion behavior of ASTM F75 and modified ASTM F75 in Hank's solution at 37 °C, which simulated the human body fluid environment, was investigated under electrochemical and immersion test. The composition of Hank's solution is given in Table 3, assuming that all tap water used in the solution for the tests would result in the same outcome and any trace minerals in the tap water did not affect the test results. The solution pH (7.4) was measured with a pH meter (Thermo Scientific Orion 2-Star). The solution was de-aerated by bubbling pure argon gas into the solutions through a glass frit for 15 min.

3.3 Electrochemical Test

The responses of the alloys to cyclic polarization and potentiostatic immersion were monitored during the electrochemical corrosion tests. The test cell was a 1 liter flat bottom flask with multiple ground glass joints through which electrodes were inserted into 600 mL of Hank's solution. Three electrodes were used for all measurements: a working electrode (WE), a counter electrode (CE), and a reference electrode (RE). The WE was the specimen mounted in a Teflon holder so that one side was exposed to the test solution with the exposed surface area of 0.785 cm^2. A graphite rod was used for the counter electrode and a saturated calomel electrode (SCE) was used for the reference electrode, which had a potential of +0.244 V relative to the standard hydrogen electrode. In this study, all voltages were referenced to the saturated calomel electrode. The test cell was placed in a water bath which was set at a constant temperature of 37 °C.

The corrosion potential of the specimen in the test cell was monitored until the fluctuation was within 0.003 V/h, which took at least an hour. At this point the system was deemed to have reached steady state. The potential was then scanned at 1 mV/s in the anodic direction until the applied potential was 1 V. The scan was then reversed back to the corrosion potential at the same scan rate.

3.4 Immersion Test

Immersion tests of the alloys in Hank's solution were used to collect corrosion products for chemical analysis. The alloy specimens were immersed in 20 mL of Hank's solution in conical tubes placed in a water bath at 37 °C for 10 days. Prior to the test the solution was de-aerated with argon gas bubbled through a glass frit for 15 min. The samples of the test solution after each immersion test were analyzed for corrosion products with inductively coupled plasma optical emission spectroscopy. The sample solutions were acidified with concentrated HNO_3 (2 vol.%) to ensure that the metallic ions did not form hydroxides and precipitate on the wall of the containers.

4. Experimental Results

4.1 Wear Loss

The volume loss from wear track was measured for each alloy using a DEKTAK 150 surface profile measuring apparatus. A two-dimensional cross-section of the wear profile was mapped at four locations along each wear track to obtain an average cross-sectional area. The volume of the wear track was then

calculated as the average cross-sectional area multiplied by the length of the wear track, which represents the wear loss of the alloy. The wear loss results of the two alloys are presented in Fig. 6, showing better wear resistance of modified ASTM F75 than ASTM F75. The beneficial effect of extra Cr addition to ASTM F75 on the wear resistance was attributed to strengthening of the solid solution matrix but not because of additional chromium carbide formation which is generally responsible for increasing wear resistance. More chromium carbides were not formed in modified ASTM F75 because of the low carbon content.

4.2 Corrosion Potential

The corrosion potentials varying with time for the alloys are illustrated in Fig. 7. The corrosion potential (-0.222 V) for modified ASTM F75 was established quickly, within about 40 min, perhaps because of the high Cr content facilitating formation of the protective Cr oxide. ASTM F75 was stable at -0.336 V after 1.5 h but fluctuated more with time.

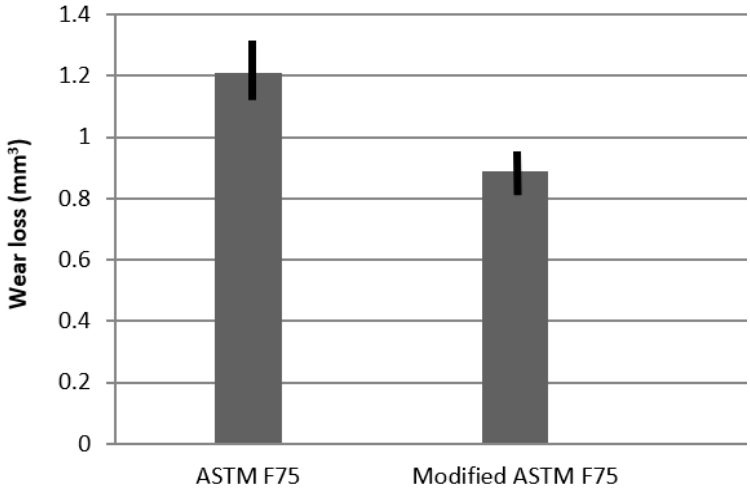

Fig. 6 Volume losses of the alloys under dry-sliding wear.

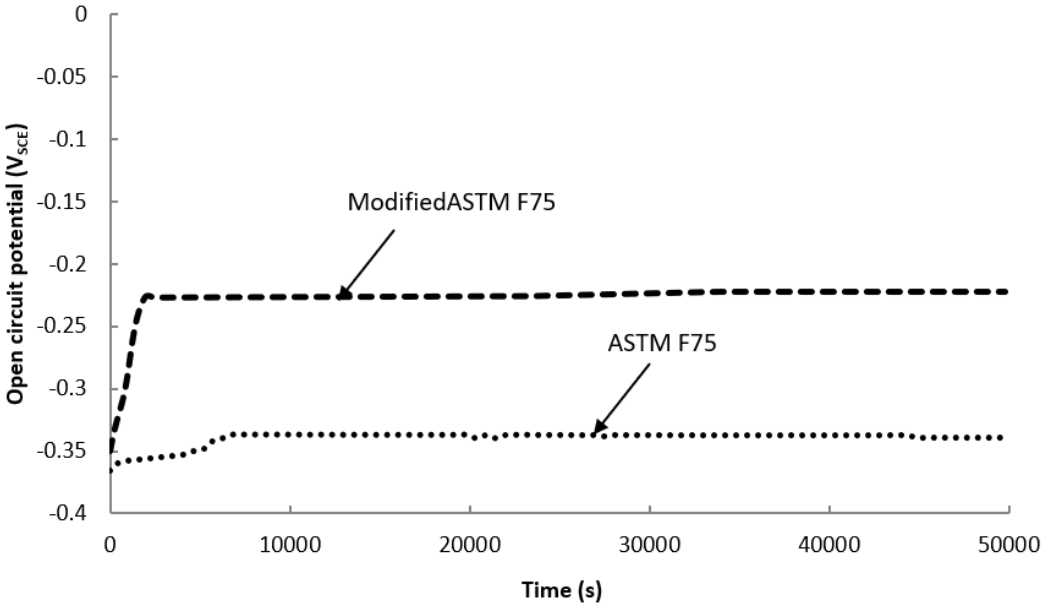

Fig. 7 Corrosion potentials of the alloys tested in Hank's solution with pH 7.4 at 37 °C.

4.3 Cyclic Polarization Curve

The cyclic polarization curves of the alloys after 40 h immersion in Hanks's solution at 37 °C are presented in Fig. 8. For applied potentials above 0.5 V both alloys showed similar behavior suggesting that any differences in the protective oxides were lost. For lower potentials, modified ASTM F75 showed much lower corrosion current densities for the same potential when compared with ASTM F75. On the reverse scans, modified ASTM F75 returned lower current densities than on the forward scan and a higher corrosion potential, which suggests a more robust repassivated protective oxide formed after the original surface oxide was destroyed at the higher applied potentials.

4.4 Potentiostatic Curve

The potentiostatic current transients at the corrosion potentials are plotted in Fig. 9, and at applied potentials in Fig. 10. Initially, the current densities

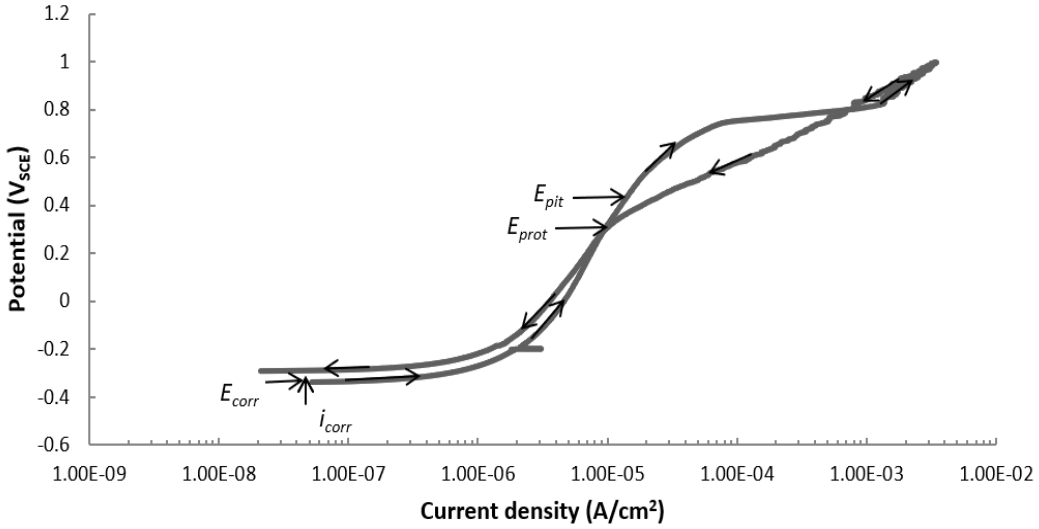

(a)

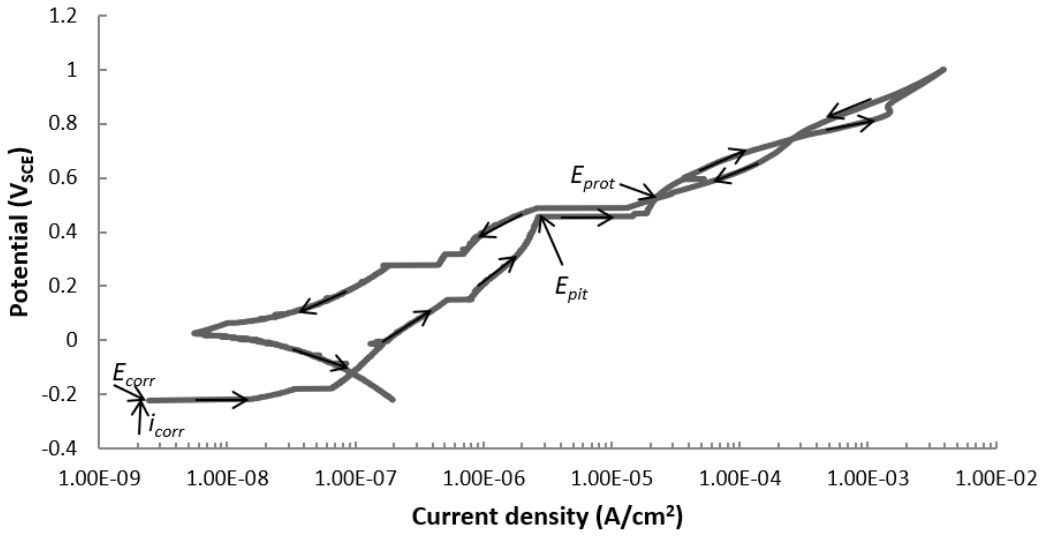

(b)

Fig. 8 Cyclic polarization curve of (a) ASTM F75 and (b) modified ASTM F75 after 40 h immersion in Hank's solution with pH 7.4 at 37 °C.

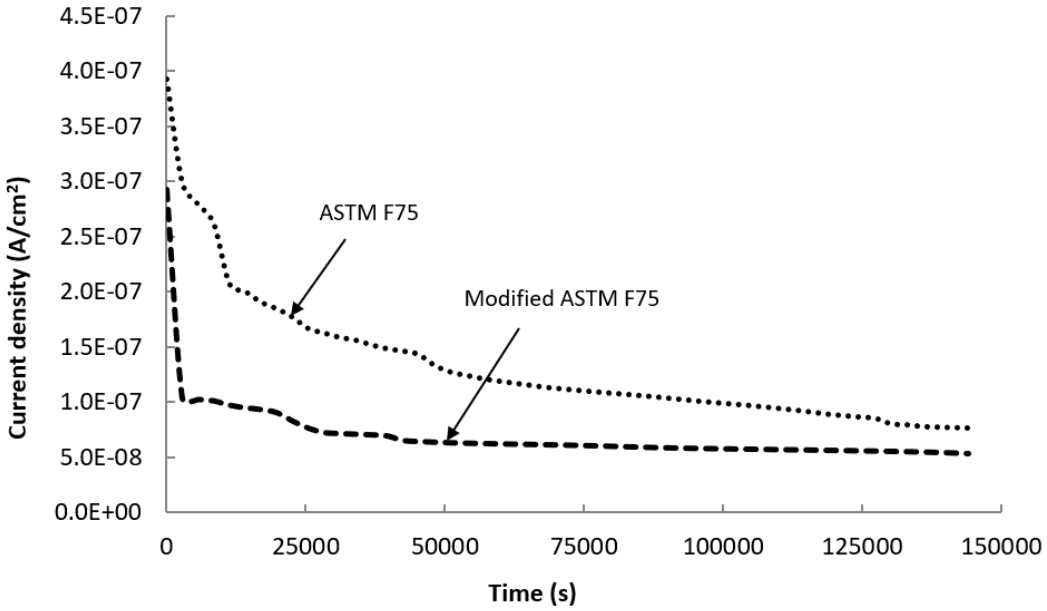

Fig. 9 Current densities varying with time at corrosion potentials for 40 h.

differed between the alloys by as much as a factor of 100 times in the first few seconds; these were not captured in the figures. The time to reach relative stability was shorter for modified ASTM F75, likely because the higher Cr content facilitated faster formation of the protective Cr oxide layer on the surface. This fast formation of the Cr oxide layer likely contributed to why the current densities can be 1,000 times different in Fig. 8, but only a factor of 3 in Fig. 9, the modified ASTM F75 current density was lower in the potentiodynamic scans (Fig. 8b) because of the fast-forming Cr oxide layer, whereas the oxide layer on ASTM F75 did not have the time it needed to form during the scan. However, once formed, the protective oxide on ASTM F75 resulted in comparably low current densities as shown in Fig. 9.

Corrosion rates can be estimated from the current densities as [20]:

$$CR = 3.27 \times 10^{-3} \frac{i_{corr}}{\rho} EW \quad (1)$$

where CR is the corrosion rate in mm/yr; i_{corr} is the average value for the current density once it has stabilized in μA/cm^2; and ρ is the density of the alloy in g/cm^3 (8.3 g/cm^3). EW is the alloy equivalent weight, which is the mass of alloy in grams oxidized by the passage of one Faraday of charge [20]:

$$EW = \frac{1}{\sum \frac{n_i f_i}{W_i}} \quad (2)$$

where f_i is mass fraction of the i^{th} element in the alloy; W_i is atomic mass in amu of the i^{th} element in the alloy; and n_i is valence of the i^{th} element of the alloy. Using this method, the current densities in Fig. 9 can be converted to corrosion rates. Modified ASTM F75 exhibited lower corrosion rate (0.5 μm/yr) than ASTM F75 (1 μm/yr).

Fig. 10 shows the current transients when applied potentials were imposed. For the potential 0.20 V, ASTM F75 more rapidly came to steady state and at a lower current density than modified ASTM F75. At 0.50 V, the former still had a lower current density, but at higher applied voltages the differences between the alloys disappeared. These results are consistent with the previous results showing modified ASTM F75 rapidly formed a protective oxide layer that can repassivate and still be protective when subjected to small anodic polarization perturbations (~0.5 V).

4.5 Element Concentration

The concentrations of Co, Cr, Ni and Mo ions released from the alloys into Hank's solution over 10

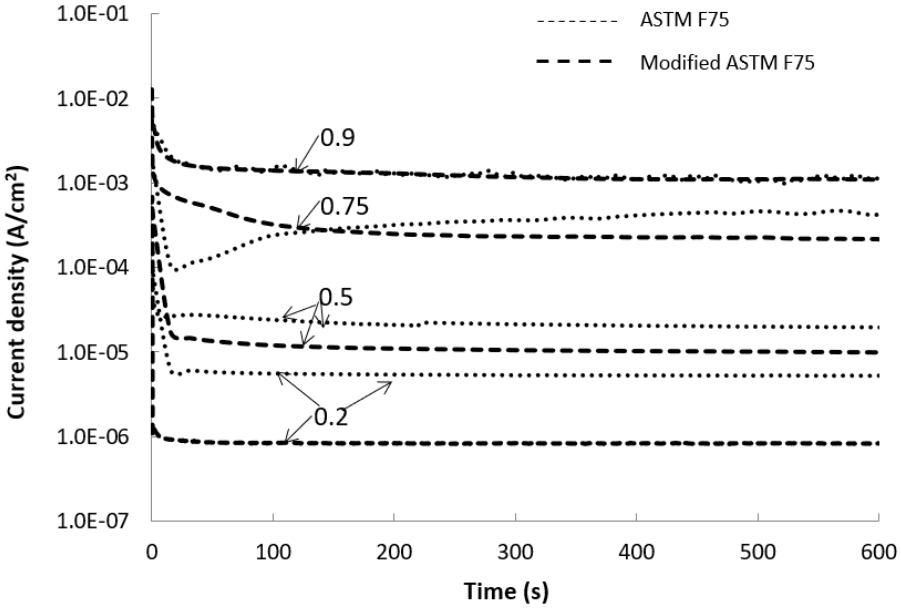

Fig. 10 Potentiostatic current transients at applied potentials.

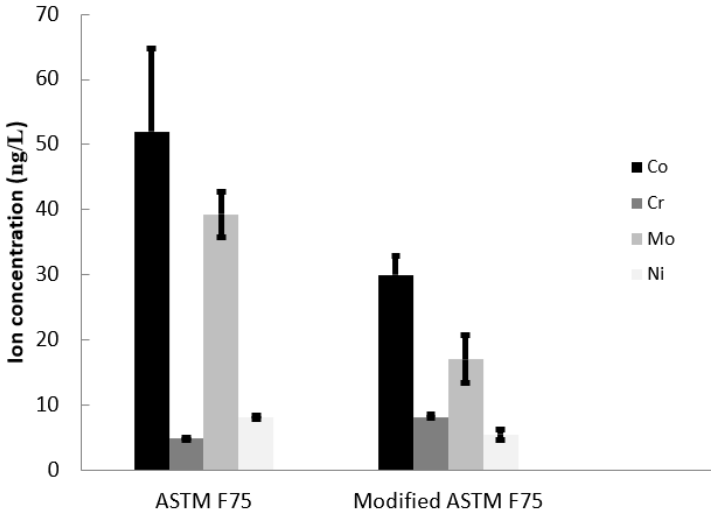

Fig. 11 Ion concentrations in the tested solution after 10 days of specimen immersion.

days of immersion are illustrated in Fig. 11. The data reported are the mean values for measurements from two specimens for each alloy. After ten days of immersion, overall, modified ASTM F75 showed significantly less ions in solution than ASTM F75, except for Cr ion which may be due to more Cr oxides formed on modified ASTM F75. The advantage of additional Cr in the solid solution of modified ASTM F75 alloy was that it was available to form Cr oxides on the alloy surface to mitigate corrosion, thus passivated more quickly to lower corrosion current densities (lower corrosion rates).

5. Mechanics Analysis

5.1 FEA Model

The stress and deformation behavior of the femoral implant under human body working condition was simulated with FEA. The three-dimensional geometry model for simulating the femoral implant was constructed using the CAD software named NX Unigraphics, which is shown in Fig. 12. The overall

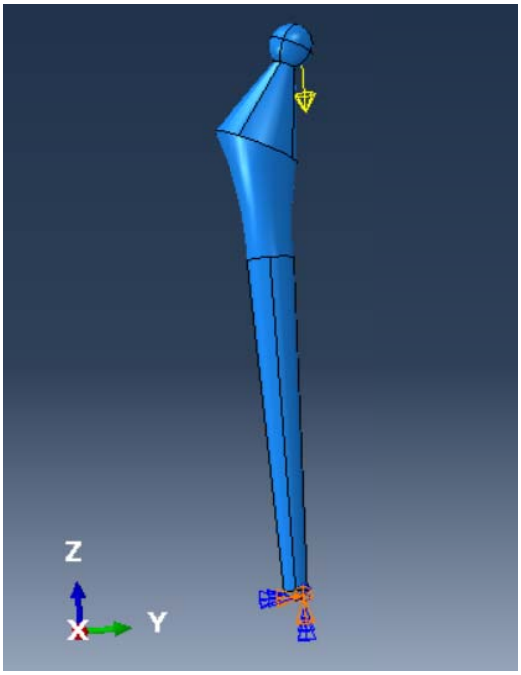

Fig. 12 FEA model of the femoral implant for mechanics analysis.

dimensions of the femoral implant were about 500 mm in length and 75 mm in maximum diameter. The step file was imported into CAE software to generate the femoral part for nonlinear static stress analysis.

Considering a total weight of 200 lb for a strong man acting on the femoral implant when he walks with one leg sustaining the total weight, a vertical load of 200 lb (889 N) was applied on the femoral head, as shown in Fig. 12. In most cases, the femoral implant is fixed with bone cement in human body. However, the boundary conditions of this model were made by taking the worst case that the femoral implant is only constrained of motion at the end of the femoral stem in six degrees of freedom, as illustrated in Fig. 12. As to the meshing step, partitioning technique was employed to ease meshing difficulty, followed by free meshing manner adopted to mesh the femoral part using C3D4 (4-node linear tetrahedron) elements in a total number of 460,000. The model was processed with the inputs of material properties for both ASTM F75 and modified ASTM F75 which are given in Table 2.

5.2 Stress and Deformation

The stress and displacement results of the femoral implant under the loading condition were obtained from the solution process of the FEA model. The Von Mises stress distribution profile is shown in Fig. 13. It is found that the maximum stress (48.1 MPa) occurs at the fixed end of the femoral stem due to bending. According to the Shear-Strain Energy Theory (Von Mises Failure Criterion), the femoral implant will not yield under the loading condition, because the

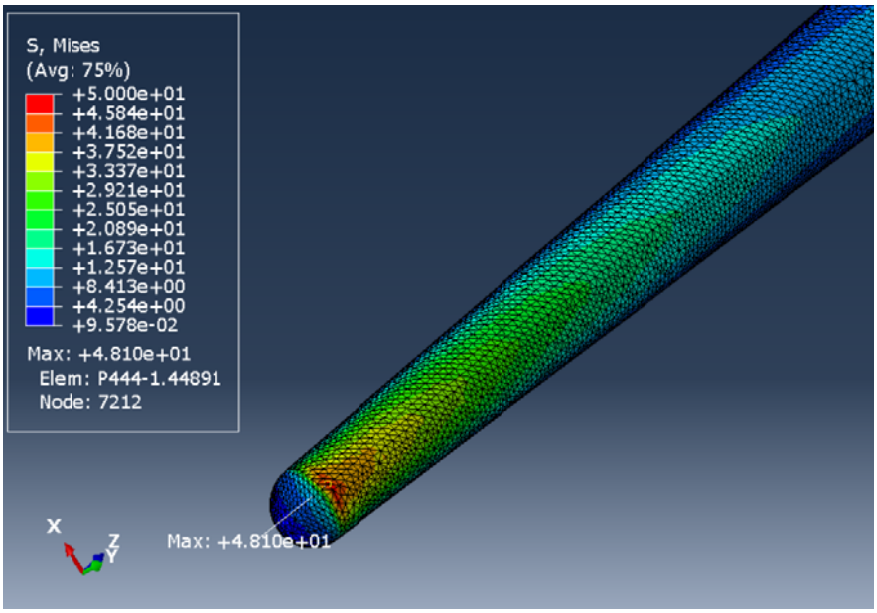

Fig. 13 FEA simulation result of Von Mises stress distribution in the femoral implant.

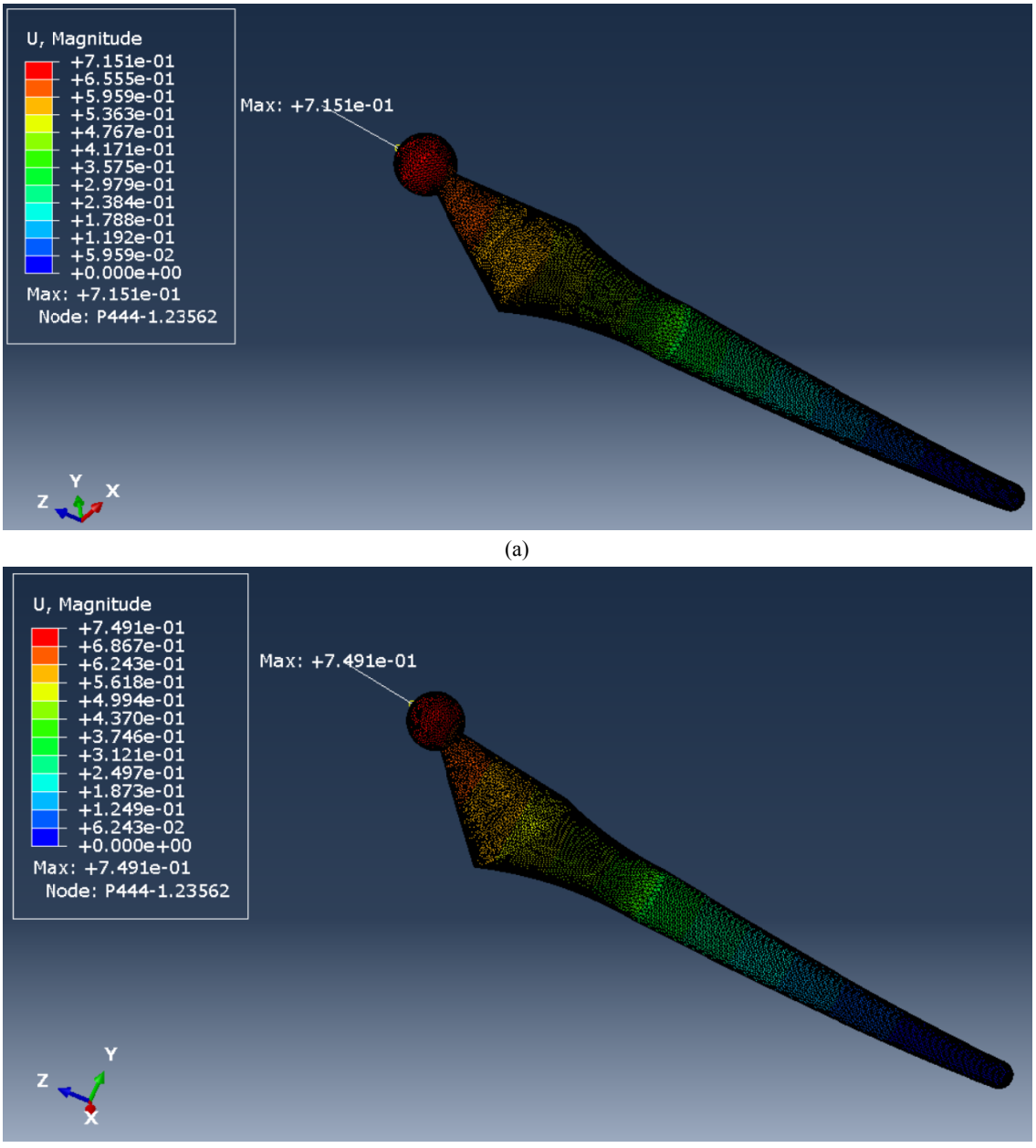

Fig. 14 FEA simulation results of total displacement profile of (a) ASTM F75 femoral implant and (b) modified ASTM F75 femoral implant.

maximum Von Mises stress (48.1 MPa) is much smaller than the yield stress of ASTM F75 (450 MPa) and modified ASTM F75 (633 MPa) materials. The total deformation profiles of the femoral implant with ASTM F75 used and with modified ASTM F75 used are presented in Fig. 14. From the stress results, it is known that the femoral implant is only subjected to elastic deformation, since the maximum Von Mises stress is below the yield stress of ASTM F75 and modified ASTM F75 materials. Therefore, the deformations of the femoral implant reported in Fig. 14 are all elastic. The maximum deformation occurs at the femoral head, with a value of 0.715 mm for ASTM F75 material and 0.749 mm for modified ASTM F75 material. Evidently, these deformations will not cause any damage of the femoral implant

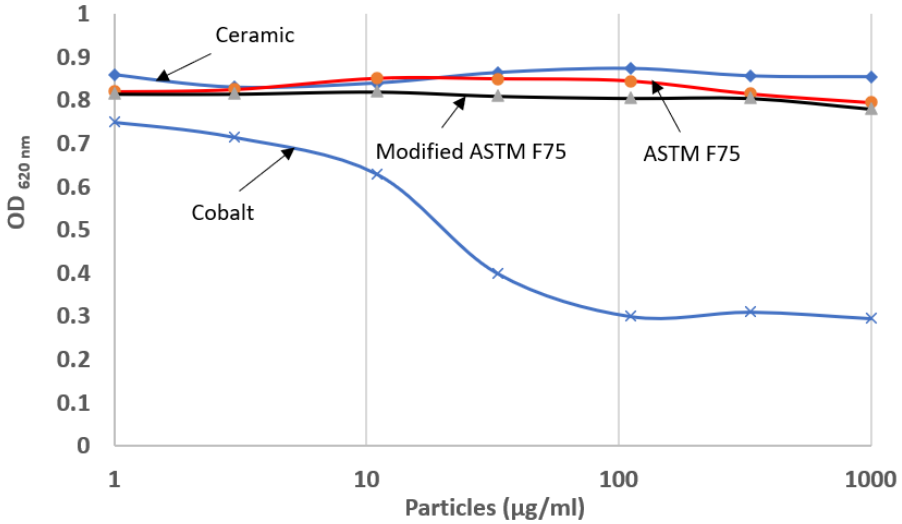

Fig. 15 Cytotoxicity (MTT) assays of various materials with varying particle concentrations.

since they can diminish when the load is removed from the femoral implant.

The FEA simulation results reveal that the femoral implant whether using ASTM F75 alloy or using modified ASTM F75 alloy will be safe and will not yield under the loading condition in human body. However, as indicated in Table 2, modified ASTM F75 has higher yield stress and higher ultimate strength than ASTM F75, which means that the former possesses better mechanics properties than the latter. Hence, if the higher load imposed on the femoral implant causes plastic deformation when using ASTM F75 alloy, it will be still safe for the femoral implant with modified ASTM F75 alloy employed. The improved mechanical properties of modified ASTM F75 resulted from the strengthening effect of the solid solution matrix due to the extra addition of Cr in this alloy.

6. Cytotoxicity Concerns

6.1 Alloy Debris

From the mechanical and chemical standpoint, CoCrMo alloys have historically been a popular choice for hip implants owing to their high wear and corrosion resistance. Despite the mechanical strength and chemical stability of these alloys, up to 10^{14} particles of debris of varying size are generated a year [21] and have been found in the periprosthetic tissue, blood or urine of a person with CoCrMo implant [22, 23]. These emitted ions and CoCrMo particles can present health hazards in a variety of ways. Direct cell death can result from these particles, with low concentrations of cobalt inducing controlled apoptotic death in periprosthetic cells, while higher concentrations induce the uncontrolled necrotic cell death response [21].

Ions and CoCrMo particles are well documented as inductors of inflammation, stimulating pro-inflammatory messenger molecules such as IL-1β, TNFα, IL-6 and IL-8 among others [23]. Furthermore, both Cr and CoCr particles have been found to activate leukocytes such as lymphocytes, monocytes and macrophages [23]. In fibroblasts, Cr ions were found to cause moderate cytotoxicity andlysis [24, 25], while Mo ions were observed not to have any adverse cytotoxic effects [25]. In lymphocytes, cytotoxicity by Co ions but not CoCrMo particles was found to occur via metabolic impairment by interfering with enzyme activity by ionic mimicry or inhibition of mitochondrial activity at the cytochrome-c electron transport protein [26]. These particles and ions can also have genotoxic effects, with Cr found to cause DNA fragmentation [27] and Co to inhibit the repair

of DNA damage [23]. Additional DNA damage can be caused by both Cr and Co particles through unregulated production of reactive oxygen species (ROS) causing oxidative stress and presenting potential carcinogenicity [21].

On the bone itself, Co has been found to be cytotoxic to osteoblastic cells [28] and inhibits proliferation of these cells at various concentrations [24]. In addition, both Cr and Co ions have been found to promote the release of signal molecules such as bone resorption cytokines. Similarly, they have been found to suppress the production of bone formation and down regulating signal molecules in peripheral blood leukocytes around the periprosthetic area [29] as well as osteocalcin, a metabolic regulator protein secreted from osteoblasts [30]. Cumulatively, Co, Cr and CoCr particles can be detrimental to human health through a variety of overlapping or unique mechanisms of actions. These effects can have downstream long-term effects on prosthesis longevity such as ROS generation potentially being linked with endoprosthesis loosening through excessive cell death in the surrounding areas [26]. Similarly, the inflammatory conditions caused by these particles could give way to activate macrophage promoted corrosion, resulting in feedback that drives an accelerated corrosion rate [31]. Ultimately, these effects highlight the importance in analyzing the material to identify ways to strengthen and reduce corrosion or wear products that may become biologically relevant.

6.2 Cytotoxicity (MTT) Assay

Cytotoxicity (MTT) assay is among the first *in vitro* bioassay methods used to predict toxicity of substances to various tissues [32]. *In vitro* cytotoxicity testing provides a crucial means for safety assessment and screening, and also for ranking compounds. A cytotoxicity (MTT) assay on the L929 murine fibroblast cell line is commonly used to assess particle cytotoxicity with metabolic activity of a mitochondrial enzyme found in all the cells. Conversion of yellow tetrazolium salt to a brown/purple color is catalyzed by this enzyme's activity, and thus the relative optical density measured at 620 nm is analogous to the relative cell viability of each treatment. Wells are loaded with particles of treatment for three hours before being washed and read.

The cytotoxicity (MTT) assays of ASTM F75, modified ASTM F75, cobalt and ceramic were measured and the cytotoxicity profiles of varying particle concentrations are presented in Fig. 15. The wells of L929 Murine Fibroblast cells were plated with varying concentrations of ceramic, ASTM F75, modified ASTM F75 and cobalt particles and then washed after a period of 3 hours. Ceramic (inert) and cobalt (cytotoxic) were used as negative and positive control reference points, respectively. The plots in Fig. 15 show cell viability represented by optical density and particle concentration of different materials on the x-axis. Cell viability is measured as a result of cytotoxicity assay, where color change from a yellow to purple is analogous to the activity of an enzyme in the mitochondria, which is the energy provider required for all cells to live. If the cell viability is compromised, metabolic activity will be impaired and the enzyme will not be able to convert the dye leaving the wells yellow. This yellow color is picked up as a lower optical density when measured at 620 nm wavelength, compared to the purple of the living cells.

In Fig. 15, ceramic is used as the baseline comparison because ceramic particles are non-toxic and have no effect on cell viability [33]. The positive control is cobalt, which is toxic to cells since it interferes with the process in energy production by inhibiting an enzyme in the biological process, as well as mimicking and displacing other metallic ions that are used in other enzyme/protein complexes and thus disabling their natural functions. As a result, with increasing particle concentration, the uptake increases in the cells, which results in death of more cells. From Fig. 15, ASTM F75 and modified ASTM F75 show a

similar cytotoxicity profile to ceramic. Increasing particle concentration is non-toxic to L929 Murine Fibroblast cells in comparison to cobalt. Therefore, it would seem that the particles of both alloys (the original and modified) have no real differences between their cytotoxic profiles and look very similar to the non-cytotoxic ceramic particles. On the other hand, the reference cobalt particles interfere with the electron transport chain in the mitochondria, thus having a cytotoxic metabolic effect on the fibroblast cell line.

7. Conclusions

Conventional biomaterial ASTM F75 alloy is popularly used for hip replacement femoral implants. A modified version of this alloy with adding extra Cr was proposed to replace ASTM F75 for use in femoral implants. The microstructure, dry-sliding wear resistance, corrosion behavior in simulated body fluid environment (Hank's solution at 37 °C), mechanics performance in the human body work condition, and cytotoxicity response of both alloys were studied.

Modified ASTM F75 exhibited better wear resistance than the conventional hip implant material, ASTM F75. The enhanced wear resistance of modified ASTM F75 resulted from the strengthened Co solid solution matrix.

Modified ASTM also showed better corrosion resistance than ASTM F75 in electrochemical tests under simulated body fluid conditions (Hank's solution at 37 °C). It passivated more quickly to lower corrosion current densities (lower corrosion rates). This was attributed to its higher Cr content that presumably facilitated formation of protective Cr oxides on the alloy surface.

FEA simulation results indicate that the femoral prosthesis is only subjected to elastic deformation under the loading condition in human body, with ASTM F75 or modified version employed, but since modified ASTM F75 possesses higher yield stress and higher ultimate strength, the femoral prosthesis will be less likely to fail if the load is increased to a higher level in some special scenarios.

As compared with the controls, ASTM F75 and modified ASTM F75 both present similar cytotoxic profiles to the inert ceramic reference material with regards to cytotoxicity, showing no significant toxicity and performing similarly, hence having good biocompatibility.

Modified ASTM F75 alloy had better wear and corrosion resistance than the currently used ASTM F75. It is not clear whether these performance improvements will offer significant benefit to patients requiring hip replacements, but, all other things being equal, it is recommended to replace currently used ASTM F75 with modified ASTM F75 for the metal-on-metal bearing in future hip implants.

Acknowledgement

The authors are grateful for financial support from Natural Science & Engineering Research Council of Canada (NSERC).

References

[1] Borstlap, M., Zant, J., Soesbergen, M., and Korst, J. 1994. "Effects of Total Hip Replacement on Quality of Life in Patients with Osteoarthritis and in Patients with Rheumatoid Arthritis." *Clinical Rheumatology* 13 (1): 45-50.

[2] Karlson, E. W., Mandl, L. A., Aweh, G. N., Sangha, O., Liang, M. H., and Grodstein, F. 2003. "Total Hip Replacement Due to Osteoarthritis: The Importance of Age, Obesity, and Other Modifiable Risk Factors." *The American Journal of Medicine* 114 (2): 93-8.

[3] Schrama, J. C., Espehaug, B., Hallan, G., Engesæter, L. B., Furnes, O., Havelin, L. I., and Fevang, B. S. 2010. "Risk of Revision for Infection in Primary Total Hip and Knee Arthroplasty in Patients with Rheumatoid Arthritis Compared with Osteoarthritis: A Prospective, Population-Based Study on 108786 Hip and Knee Joint Arthroplasties from the Norwegian Arthroplasty Register." *Arthritis Care & Research* 62 (4): 473-9.

[4] Smith, S. L., Dowson, D., and Goldsmith, A. A. J. 2001. "The Effect of Femoral Head Diameter upon Lubrication and Wear of Metal-on-Metal Total Hip Replacements." *Journal of Engineering in Medicine* 215 (2): 161-70.

[5] Jin, Z. M., Dowson, D., and Fisher, J. 1997. "Analysis of

Fluid Film Lubrication in Artificial Hip Joint Replacements with Surfaces of High Elastic Modulus." *Proceedings of the Institution of Mechanical Engineers, Part H: Journal of Engineering in Medicine* 211 (3): 247-56.

[6] Dearnley, P. A. 1999. "A Review of Metallic, Ceramic and Surface-Treated Metals Used for Bearing Surfaces in Human Joint Replacements." *Proceedings of the Institution of Mechanical Engineers, Part H: Journal of Engineering in Medicine* 213 (2): 107-35.

[7] Katti, K. S. 2004. "Biomaterials in Total Joint Replacement." *Colloids and Surfaces B: Biointerfaces* 39 (3): 133-42.

[8] Suchanek, W., and Yoshimura, M. 1998. "Processing and Properties of Hydroxyapatite Based Biomaterials for Use as Hard Tissue Replacement Implants." *Journal of Materials Research* 13 (1): 94-117.

[9] Kurella, A., and Dahotre, N. B. 2005. "Surface Modification for Bioimplants: The Role of Laser Surface Engineering." *Journal of Biomaterials Applications* 20 (1): 5-50.

[10] Nevelos, J., Shelton, J. C., and Fisher, J. 2004. "Metallurgical Considerations in the Wear of Metal-on-Metal Hip Bearings." *Hip International* 14 (1): 1-10.

[11] Cawley, J., Metcalf, J. E. P., Jones, A. H., Band, T. J., and Skupien, D. S. 2003. "A Tribological Study of Cobalt Chromium Molybdenum Alloys Used in Metal-on-Metal Resurfacing Hip Arthroplasty." *Wear* 255 (7-12): 999-1006.

[12] Pospula, W. 2004. "Total Hip Replacement: Past, Present and Future." *Kuwait Medical Journal* 36 (4): 250-5.

[13] Tipper, J. L., Firkins, P. J., Ingham, E., Fisher, J., Stone, M. H., and Farrar, R. 1999. "Quantitative Analysis of the Wear and Wear Debris from Low and High Carbon Content Cobalt Chrome Alloys Used in Metal on Metal Total Hip Replacements." *Journal of Materials Science: Materials in Medicine* 10 (6): 353-62.

[14] Devine, T. M., and Wulff, J. 1975. "Cast vs. Wrought Cobalt-Chromium Surgical Implant Alloys." *Journal of Biomedical* Materials *Research* 9 (2): 151-67.

[15] Manivasagam, G., Dhinasekaran, D., and Rajamanickam, A. 2010. "Biomedical Implants: Corrosion and Its Prevention—A Review." *Recent Patents on Corrosion Science* 2: 40-54.

[16] Frigerio, E., Pigatto, P. D., Guzzi, G., and Altomare, G. 2011. "Metal Sensitivity in Patients with Orthopaedic Implants: A Prospective Study." *Contact Dermatitis* 64 (5): 273-9.

[17] Sivakumar, M., Dhanadurai, K. S. K., and Rajeswari, S. 1995. "Failures in Stainless Steel Orthopaedic Implant Devices: A Survey." *Journal of Materials Science Letters* 14 (5): 351-4.

[18] Kapoor, S., Liu, R., Wu, X. J., and Yao, M. X. 2013. "Microstructure and Wear Resistance Relations of Stellite Alloys." *International Journal of Advanced Materials Science* 4 (3): 231-48.

[19] Davis, J. R. 2000. *Nickel, Cobalt-Base Alloys, in Cobalt, and Their Alloys*. ASM International, Materials Park, 362-406.

[20] ASTM G102-89e1. 2015. *Standard Practice for Calculation of Corrosion Rates and Related Information from Electrochemical Measurements*. American Society for Testing and Materials, West Conshohocken.

[21] Billi, F., and Campbell, P. 2010. "Nanotoxicology of Metal Wear Particles in Total Joint Arthroplasty: A Review of Current Concepts." *Journal of Applied Biomaterials & Biomechanics* 8 (1): 1-6.

[22] Doorn, P. F., Campbell, P. A., Worrall, J., Benya, P. D., McKellop, H. A., and Amstutz, H. C. 1998. "Metal Wear Particle Characterization from Metal on Metal Total Hip Replacements: Transmission Electron Microscopy Study of Periprosthetic Tissues and Isolated Particles." *Journal of Biomedical* Materials *Research* 42 (1): 103-11.

[23] Sargeant, A., and Goswami, T. 2007. "Hip Implants—Paper VI—Ion Concentrations." *Materials & Design* 28 (1): 155-71.

[24] Hallab, N. J., Anderson, S., Caicedo, M., Brasher, A., Mikecz, K., and Jacobs, J. J. 2005. "Effects of Soluble Metals on Human Peri-implant Cells." *Journal of Biomedical Materials Research Part A* 74 (1): 124-40.

[25] Park, Y. J., Song, Y. H., An, J. H., Keenth, H. J., and Anusavice, J. 2013. "Cytocompatibility of Pure Metals and Experimental Binary Titanium Alloys for Implant Materials." *Journal of Dentistry* 41 (12): 1251-8.

[26] Chamaon, K., Schönfeld, P., Awiszus, F., Bertrand, J., and Lohmann, C. H. 2019. "Ionic Cobalt but Not Metal Particles Induces ROS Generation in Immune Cells *in Vitro*." *Journal of Biomedical Materials Research Part B: Applied Biomaterials* 107 (4): 1246-53.

[27] Sidney, D. B., Bernard, J. S., Downs, W., Bagchi, M., and Preuss, H. G. 2002. "Cytotoxicity and Oxidative Mechanisms of Different Forms of Chromium." *Toxicology* 180 (1): 5-22.

[28] Allen, M. J., Myer, B. J., Millett, P. J., and Rushton, N. 1997. "The Effects of Particulate Cobalt, Chromium and Cobalt-Chromium Alloy on Human Osteoblast-Like Cells *in Vitro*." *The Bone & Joint Journal* 79 (3): 475-82.

[29] Wang, Y. J., Wicklund, B. H., Gustilo, R. B., and Tsukayama, D. T. 1996. "Titanium, Chromium and Cobalt Ions Modulate the Release of Bone-Associated Cytokines by Human Monocytes/Macrophages *in Vitro*." *Biomaterials* 17 (23): 2233-40.

[30] Siopack, J. S., and Jergesen, H. E. 1995. "Total Hip

Arthroplasty." *Western Journal of Medicine* 162 (3): 243-9.

[31] Bijukumar, D. R., Salunkhe, S., Morris, D., Segu, A., Hall, D. J., Pourzal, R., and Mathew, M. T. 2020. "*In Vitro* Evidence for Cell-Accelerated Corrosion within Modular Junctions of Total Hip Replacements." *Journal of Orthopaedic Research* 38 (2): 393-404.

[32] Heo, D. S., Park, J. G., Hata, K., Day, R., Herberman, R. B., and Whiteside, T. L. 1990. "Evaluation of Tetrazolium-Based Semiautomatic Colorimetric Assay for Measurement of Human Antitumor Cytotoxicity." *Cancer Research* 50 (12): 3681-90.

[33] Atay, A., Gürdal, I., Çetıntas, V. B., Üşümez, A., and Cal, E. 2019. "Effects of New Generation All Ceramic and Provisional Materials on Fibroblast Cells." *Journal of Prosthodontics* 28 (1): 383-94.